RSC Advances

PAPER

View Article Online
View Journal | View Issue

Cite this: *RSC Adv.*, 2021, **11**, 22014

UV cross-linked smart microgel membranes as free-standing diffusion barriers and nanoparticle bearing catalytic films†

Maxim Dirksen, [a] Timo Brändel, [a] Sören Großkopf,[a] Sebastian Knust, [b] Johannes Bookhold,[a] Dario Anselmetti [b] and Thomas Hellweg *[a]

In this study we use poly(*N*-isopropylacrylamide) (PNIPAM) based copolymer microgels to create free-standing, transferable, thermoresponsive membranes. The microgels are synthesized by copolymerization of NIPAM with 2-hydroxy-4-(methacryloyloxy)–benzophenone (HMABP) and spin-coated on Si wafers. After subsequent cross-linking by UV-irradiation, the formed layers easily detach from the supporting material. We obtain free standing microgel membranes with lateral extensions of several millimetres and an average layer thickness of a few hundred nanometres. They can be transferred to other substrates. As one example for potential applications we investigate the temperature dependent ion transport through the membranes *via* resistance measurements revealing a sharp reversible increase in resistance when the lower critical solution temperature of the copolymer microgels is reached. In addition, prior to cross-linking, the microgels can be decorated with silver nanoparticles and cross-linked afterwards. Such free-standing nanoparticle hybrid membranes are then used as catalytic systems for the reduction of 4-nitrophenol, which is monitored by UV/Vis spectroscopy.

Received 6th May 2021
Accepted 15th June 2021

DOI: 10.1039/d1ra03528b

rsc.li/rsc-advances

1 Introduction

Modern developments in membrane technology are aiming at fabrication of interactive membranes with tailored functionality,[1] superior mechanical properties,[2] controlled pore size,[3] switching capability,[4] and ability to respond to environmental stimuli.[5–7] Especially responsive nano-membranes are promising materials for nanotechnology,[8] because they can be used for a variety of applications like the separation of gases,[9,10] as carriers for catalysts,[11] for chromatography[12,13] or in cell culture applications for vertebrate cells.[14]

Many of these responsive membranes are fabricated with stimuli-responsive polymers which are used to make macroscopic hydrogel sheets[7] or to functionalize other non-responsive membranes.[15] One of the most prominent examples for responsive polymer materials are thermoresponsive microgels based on poly-(*N*-isopropylacrylamide) (PNIPAM).[16–19] It is well known, that PNIPAM microgels are swollen with water at temperatures below the volume phase transition temperature (VPTT) of 33 °C.[20] An increase of the temperature causes a microphase separation towards a collapsed state accompanied by a significant change in particle size.[16,21] Due to their fascinating behaviour stimuli-responsive microgels are candidates for applications such as uptake and release,[22,23] diffusion control of small and large molecules,[21,24] drug delivery,[25–27] sensors[28,29] or as nanoparticle carriers.[30,31] The mentioned phase behaviour is also exploited to control catalytic activity of noble metal nanoparticles inside the polymer network.[32] Moreover, PNIPAM based microgels can easily be copolymerized to tailor their properties.[33–35] One of the major drawbacks concerning all those applications of microgels is the purification, as the microgels usually have to be removed after any kind of process.[32] It could be very advantageous if *e.g.* catalytic reactions could be performed in a flow-through device.

One possibility to overcome this issue is to functionalize surfaces with thermoresponsive microgels by coating them *via* different methods such as spin-coating or spray-coating. For instance, spin-coating gave good results in cell-culture applications.[36,37] To prepare functionalized membranes, nowadays usually porous organic or inorganic membranes are subsequently modified with linear PNIPAM chains or with PNIPAM based microgels.[38–45] However, all these approaches require multiple-step procedures and are limited to commercially available supports for functionalization. In contrast to that, a free-standing cross-linked microgel film or membrane would offer many advantages for surface modifications, especially when three-dimensional objects or wells should be coated or wrapped. This issue is, according to our experience, hardly

[a]*Department of Chemistry, Physical and Biophysical Chemistry, University Bielefeld, Universitätsstraße 25, D-33615 Bielefeld, Germany. E-mail: thomas.hellweg@uni-bielefeld.de; Fax: +49 521-106-2981; Tel: +49 521-106-2055*

[b]*Department of Physics, Experimental Biophysics, University Bielefeld, Universitätsstraße 25, D-33615 Bielefeld, Germany*

† This work is dedicated to my colleague and friend Karl Kratz who passed away by far too early at the beginning of 2021. About 25 years ago Karl introduced me to microgel research and we did several joint neutron scattering experiments on his samples which led to very important publications in the field of microgels. I will always be grateful to him.

achievable with spin-coating.[38,46] Hence, the present work is addressed towards this and describes a suitable method to develop free-standing cross-linked microgel films, to use them as diffusion barriers, to control ion flux or as catalytic membranes.

A good access towards free-standing microgel membranes is the irreversible cross-linking of single microgel particles to a layer, which can be realized by different approaches. One possibility is electron beam cross-linking of microgel particles. This principle has been presented by Bookhold *et al.*, recently.[47] In this work Bookhold *et al.* applied the idea of cross-linking microgel particles by electron beam irradiation inspired by the work of Gölzhäuser *et al.* on cross-linking of self-assembled monolayers.[6,48,49] The electron beam cross-linked microgel membranes showed a reversible thermoresponsive behaviour and were free-standing microgel monolayers with a thickness below 100 nm in the dry state. However, there is some uncertainty related to the chemical details of the cross-linking process related to the high electron energy. In addition, the used preparation scheme is quite invasive, since for the detaching of free-standing microgel films, aqua regia was used to dissolve the substrate.

In order to present a less invasive method, in this work we have decided to use UV-light for cross-linking microgel particles. This method has already been successfully used in the fabrication of various 2D materials such as photo resists coatings in semiconductor device production.[50–53] For this, as in the case of electron beam cross-linking, the incorporation of a cross-linkable aromatic comonomer, which is 2-hydroxy-4-(methacryloyloxy)–benzophenone (HMABP), is of great importance, since only in this way sufficient cross-linking of the particles is achieved. Moreover, UV cross-linking hardly needs effort compared to electron beam cross-linking and the layers can be easily detached without the use of strong acids and transferred to any substrate. We synthesized PNIPAM based microgels with different HMABP contents and investigated the incorporation of the aromatic comonomer by means of NMR spectroscopy. Additionally the size and swelling behaviour of the microgel particles was investigated with different scattering techniques like small angle X-ray scattering (SAXS) and photon correlation spectroscopy (PCS).

The microgel particles were UV cross-linked and the obtained free-standing membranes were analyzed with atomic force microscopy (AFM) and ellipsometry. To investigate the thermoresponsive behaviour of the free-standing membranes, we performed temperature dependent resistance measurements in a custom designed microfluidic device. And finally as a proof of concept, we fabricated free-standing microgel membranes, which are decorated with silver nanoparticles and showed that these membranes can be used as catalysts for the reduction of 4-nitrophenol.

2 Experimental

2.1 Materials

N-Isopropylacrylamide (NIPAM, TCI Germany GmbH, Eschborn, Germany; 97%) was recrystallized from *n*-hexane (p.a., VWR International, Eschborn, Germany). 2-Hydroxy-4-(methacryloyloxy)–benzophenone (HMABP, Alfa Aesar, Karlsruhe, Germany; 99%), *N*,*N*′-methylenbisacrylamide (BIS, Sigma Aldrich, Munich, Germany; 99%), sodium dodecyl sulfate (SDS, Sigma Aldrich, Munich, Germany; 99%), ammonium persulfate (APS, Sigma Aldrich, Munich, Germany; ≥99%), sodium hydroxide (p.a., 0.1 M, VWR International, Eschborn, Germany), *N*,*N*-dimethylformamide-d_7 (DMF-d_7, DEUTERO GMBH, Kastellaun, Germany; ≥99.5 atom%), silver nitrate (Sigma Aldrich, Munich, Germany; 99.999%), 4-nitrophenol (Carl Roth, Karlsruhe, Germany; 99%) and sodium borohydride (Sigma Aldrich, Munich, Germany; 98.0%) were used without further purification. Water was purified using an Arium pro VF system (Sartorius AG, Göttingen, Germany).

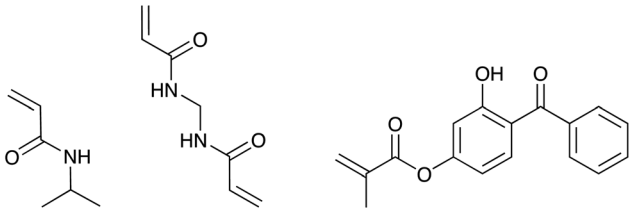

Fig. 1 Chemical formulae of the monomers used for the microgel syntheses (left to right: *N*-isopropylacrylamide (NIPAM), *N*,*N*′-methylenebisacrylamide (BIS) and 2-hydroxy-4-(methacryloyloxy)-benzophenone (HMABP)).

2.2 Synthesis of the copolymer microgels

The copolymer microgels PNIPAM-*co*-HMABP were synthesized *via* the classical Pelton synthesis approach.[54] For all syntheses the amount of the monomer NIPAM and the cross-linker BIS was kept constant and the UV-sensitive comonomer HMABP was used in different molar amounts with respect to the thermoresponsive material. The chemical structures of the used monomers are presented in Fig. 1.

In a typical synthesis NIPAM (0.6535 g, 5.77 mmol), BIS (0.0445 g, 0.289 mmol, 5 mol%) and SDS (0.0149 g, 0.69 mmol L^{-1} synthesis concentration) were dissolved in 69 mL of purified water. The solution was heated up by an oil bath (80 °C) under continuous stirring (400 rpm) and purged with nitrogen for 1 h. Simultaneously HMABP (total amounts are listed in Table 1) was dissolved in 5 mL of purified water, treated with an ultrasonic bath and added to the reaction solution. The polymerization was initiated by the addition of APS (0.0463 g, 0.202 mmol, 3.5 mol%) dissolved in 1 mL purified water and was left to proceed for 4 h at an oil bath temperature of 80 °C. Afterwards the reaction solution was cooled down to room temperature and stirred overnight. All microgels were purified

Table 1 Composition of the different microgels and the feeds of the comonomer HMABP

Sample name	mol%	Monomer feed/ mmol	Mass/g
NcHMABP2.5	2.5	0.145	0.0408
NcHMABP5	5	0.289	0.0861
NcHMABP10	10	0.577	0.1629
NcHMABP15	15	0.865	0.2443

Table 2 Optimized spin-coating protocols for coating the wafers with the respective microgels. In summary, the concentrations of the microgel solutions, the waiting time before the start of the spin-coating routine, the repetition of the procedure and the rotation speed are listed

Sample	wt%	Waiting/min	Rot. speed/rpm	Repetition
NcHMABP2.5	1.12	10	1000	3
NcHMABP5	0.7	10	1000	3
NcHMABP10	1.2	10	1500	3
NcHMABP15	1.4	15	1000	3

by 5 successive centrifugation, decantation and redispersion cycles with purified water.

2.3 Preparation of free-standing microgel layers

The fabrication of the free-standing cross-linked microgel layers is accomplished by means of an optimized spin-coating procedure and subsequent irradiation of the layer with UV-light. For this purpose individually optimized spin-coating procedures (see Table 2) were developed using a spin-coater (Süss MicroTec Lithography GmbH) in order that a dense packing of the respective microgel particles on the surface was achieved. The quality of the coating was controlled by AFM measurements. Furthermore, the layer thickness was optimized so that a stable microgel film could be obtained after cross-linking. For cross-linking the layers were irradiated with an UV-lamp (400 W, Polimer 400, Ielios Italquartz S.r.l., Milano, Italy) for 120 s. Finally the coated substrate was immersed in a 0.1 M NaOH solution. After waiting for 30 s, the substrate was transferred to a vessel filled with purified water. There, the cross-linked layer separates from the substrate and floats to the air–water interface, where it is transferred to a silicon nitride chip (Si_3N_4, 3 × 3 mm, membrane window: 70 × 70 μm^2, Silson Ltd, Southam, GB) for further resistance measurements.

2.4 NMR spectroscopy

To study the percentage of incorporation of HMABP in the respective microgels, ^{1}H-NMR spectra were recorded. For this purpose a FT-NMR spectrometer (Avance III 500, Bruker Corporation, Billerica, Massachusetts) was used. The microgels were freeze-dried for 24 h and 5 mg of each sample were dissolved in DMF-d_7. All measurements were done at 500 MHz and 1024 scans. For the calculation of the relative incorporation of the aromatic comonomer, the integrals for the isopropyl proton of NIPAM (3.7–4.3 ppm) were set in relation to the integrals of the aromatic component of HMABP (6.8–7.9 ppm).

2.5 Photon correlation spectroscopy (PCS)

The temperature-dependent determination of the hydrodynamic radius was performed using a HeNe laser with an ALV-6010/E multiple-τ digital correlator at a constant scattering angle of 60°. To avoid multiple scattering, the concentration of the solution was below 0.0002 wt%. The temperature was adjusted using a thermostated decaline bath. The temperature-dependent phase behaviour was investigated in a temperature range of 10–50 °C. At each temperature the sample was allowed to equilibrate for 25 min. The resulting auto-correlation functions were analyzed by inverse Laplace transformation using CONTIN to obtain the mean relaxation rate $\bar{\Gamma}$.[55] *Via* $\bar{\Gamma} = D^T \cdot q^2$ the translational diffusion coefficient D^T can be calculated with q as magnitude of the scattering vector ($q = |\vec{q}| = \frac{4\pi n}{\lambda} \cdot \sin\left(\frac{\theta}{2}\right)$, with λ being the wavelength of the scattered light, n the refractive index of the solvent and θ the scattering angle). Furthermore, using the Stokes–Einstein relation (eqn (1)), a calculation of the hydrodynamic radius R_h of the microgel particles is possible:

$$D^T = \frac{k_b T}{6\pi\eta R_h} \quad (1)$$

here, k_b is the Boltzmann constant, T the temperature and η the corresponding viscosity of the sample. To obtain the volume phase transition temperature (VPTT) for the respective microgels the point of inflection of the swelling curves was determined using the same approach as in previous works.[27]

2.6 Small-angle X-ray scattering (SAXS)

SAXS experiments were performed at 40 °C on an inhouse SAXS/WAXS system (XEUSS, Xenocs, Sassenage, France) with a CuK_α source (λ = 1.541 Å, GeniX Ultra low divergence, Xenocs, Sassenage, France) and a Pilatus 300K hybrid pixel detector (Dectris, Baden Deattwil, Switzerland) to investigate the effect of incorporation of HMABP on the particle structure. The covered q-range was 0.005 to 0.035 Å^{-1}. The data were analyzed using the Foxtrot software (Version 3.3.4, G. Viguier, R. Girardot). The samples were normalized to incident intensity, sample thickness, measuring time, transmission and background. The scattered intensity was brought to absolute scale using glassy carbon (type 2, sample P11).[56] In small-angle X-ray scattering experiments, the scattered intensity

$$I(q) = N \cdot I_0 \cdot \Delta\rho^2 \cdot V^2 \cdot P(q) \cdot S(q) \quad (2)$$

is dependent on the number of particles N, the incident intensity I_0, the scattering volume of the sample V, the electron density difference $\Delta\rho = \rho_{particle} - \rho_{solvent}$, on the particle form factor $P(q)$, and the structure factor $S(q)$. Here, the magnitude of the scattering vector is defined as

$$q = \frac{4\pi}{\lambda} \cdot \sin\left(\frac{\theta}{2}\right) \quad (3)$$

at a scattering angle of θ. For dilute solutions $S(q) \approx 1$ and only the form factor has to be considered. Hence, the obtained data were fitted using the homogeneous sphere model (eqn (4)) implemented in SasView.[57,58] The form factor of the sphere is convoluted with a Gaussian distribution of the radius to account for polydispersity. The model describes the scattering intensity $I(q)$ as a function of the concentration of the spherical objects $\phi_{spheres}$, the volume of the scattering sphere v, the radius of the sphere r, the background b, and the scattering length difference between the scatterer and the solvent $\Delta\rho$.

$$I(q) = (\Delta\rho)^2 \phi_{spheres} v \left(3\frac{\sin(qr) - qr\cos(qr)}{(qr)^3}\right)^2 + b \quad (4)$$

2.7 Atomic force microscopy (AFM)

Atomic force microscopy (AFM) was used to investigate the cross-linked microgel layers on the substrates. First and foremost the layers were investigated for homogeneity and high packing density in order to exclude any defects. The measurements were performed with a DI Nanoscope IIIa (Digital Instruments, now Bruker, Karlsruhe, Germany) mounted on a Zeiss Axiovert 135 inverted microscope (Carl Zeiss Microscopy GmbH, Jena, Germany) in semi-contact mode using Budget Sensors (Innovative Solution Bulgaria Ltd, Sofia, Bulgaria) Al-Reflex Tap300Al-G cantilevers with a tip radius of <10 nm, a resonance frequency of about 300 kHz and a spring constant of 40 N m^{-1}. In addition, the surface roughness of the layers was determined using the software Gwyddion.[59]

2.8 Ellipsometry

Ellipsometry measurements were performed to investigate the layer thickness of the cross-linked microgels on a substrate in the dried state using a single-wavelength ellipsometer (SE 400adv, SENTECH Instruments GmbH, Berlin, Germany). The method of ellipsometry is described elsewhere.[60,61] The measurements were controlled with the software SE400advanced from SENTECH. For modeling, a first guess of the microgel layer thickness based on the AFM measurements of one spin-coating procedure was used. The initial refractive index was estimated based on literature to 1.35.[62]

2.9 Resistance measurements

The resistance measurements were performed using a custom designed microfluidic device made of two plexiglass blocks (Fig. 2) to investigate the reversible temperature-dependent switching behaviour of the membranes. Each block contains a reservoir for the electrolyte solution (green). The contact between the reservoirs is given by a narrow channel. As in our earlier work, the detached microgel membranes were transferred to Si_3N_4 chips with a funnel hole.[47] Subsequently, the Si_3N_4 chip with the microgel membrane is placed between the two blocks with a PDMS seal. The depth of the window corresponds to the thickness of the chip, allowing precise and damage-free placement. To ensure accurate temperature control during the measurement, each block has a cooling channel (blue) that runs as close as possible to the reservoir and the transverse bore. The temperature of the cooling medium is controlled by a thermostat (Huber, Microprocessor Control MPC E, Kältemaschinenbau AG, Offenburg, Germany). Subsequently, the exact temperature of the cooling medium is detected by a Pt-1000 temperature sensor (black) and read out *via* a microvoltmeter Keithley 197 (Keithley Instruments, Autoranging Microvolt DMM, Cleveland, Ohio, USA) using a LabView program. For preparation both blocks were dipped into a degassed phosphate buffer solution (20 mM KCl, 20 mM sodium dihydrogenphosphate, pH = 7) to exclude bubble formation in the measuring channel while filling the reservoirs. Then the chip was placed at the intended position and both blocks were joined by screws. The entire preparation takes place in the buffer solution. To avoid interference from the outside, the measurements were carried out in a Faraday cage. The electrical contacting was done using two Ag/AgCl electrodes. The resistance as a function of temperature was measured in a temperature range of 15 °C to 40 °C and employing a voltage of ±5 mV using an Axopatch 200B Amplifier (Molecular Devices, Biberach, Germany).

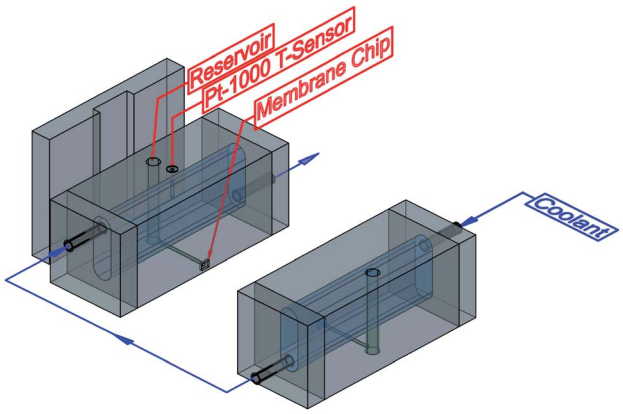

Fig. 2 Schematic representation of the microfluidic device developed for the resistance measurements. The cooling channel is shown in blue, the reservoirs for the electrolytic solution in green and the temperature sensor, as well as the connections for the thermostat are shown in black. The cooling circuit is indicated by blue arrows.

2.10 Synthesis of silver nanoparticles

Silver nanoparticles were synthesized inside copolymer microgel particles with a HMABP content of 5 mol%. Therefore 5 mL of the microgel suspension were mixed with 0.26 mL of a 0.1 M silver nitrate solution. The reaction mixture was equilibrated with an ice bath under constant nitrogen flux and stirring for 30 min. After that 1 mL of a freshly prepared, aqueous sodium borohydride solution (0.5 M) was added slowly to the reaction mixture. The mixture was allowed to reach room temperature afterwards. For the purification the reaction solution was dialyzed against 500 mL of water for 48 h. The water was changed five times during the dialysis procedure.

2.11 Transmission electron microscopy (TEM)

TEM samples of the Ag-nanoparticle/microgel hybrids were prepared by dropping 3 μL of a highly diluted sample solution on a carbon coated copper grid (ECF200-Cu, 200 mesh, Science Services, Munich, Germany) for 1 min and afterwards the residual water was blotted off with a filter paper. The TEM grids have been made hydrophilic before by plasma treatment with air. The samples were imaged in a Phillips CM100 electron microscope (FEI Deutschland GmbH, Dreieich, Germany) equipped with a tungsten electron gun to investigate the incorporation of silver nanoparticles into the microgels. The TEM was operated at an acceleration voltage of 80 kV. The images were recorded digitally by a bottom-mounted CCD camera. To achieve good statistics several positions on each grid were imaged.

2.12 Catalysis measurements

The catalytic activity of the free-standing membranes with silver nanoparticles was measured using an Agilent 8453 UV/Vis

spectrometer (Agilent Technologies Germany, Ratingen, Germany) equipped with a diode-array detector. The eight-position sample holder was set to a temperature of 40 °C and controlled by a water thermostat (Haake Phoenix II, Thermo Haake GmbH, Karlsruhe, Germany). The respective membrane was transferred into a Hellma sample cell (Hellma GmbH, Mühlheim, Germany) and resuspended in 2.0 mL of a 0.05 mM 4-nitrophenol solution. After an equilibration time of 30 min the reaction was started by adding 20 μL of a $NaBH_4$-solution (0.028 g mL^{-1}) and a full absorption spectrum of the sample was acquired from 190–1100 nm every 30 s for 6000 s.

3 Results and discussion

3.1 Comonomer incorporation

For the cross-linking of the microgel particles into a free-standing membrane, the incorporation of the comonomer is the most important parameter.

The determination of the incorporated amount of HMABP was performed by NMR spectroscopy (see Fig. 3). To obtain the relative HMABP content in relation to the thermoresponsive material (NIPAM) the integrals of the proton corresponding to the isopropyl group and the protons corresponding to the aromatic moiety were used (red boxes). Fig. 3 shows, that the copolymerization of NIPAM with the UV-sensitive comonomer was carried out successfully in all cases, as shown in the aromatic region (see left red box) where the intensity of the signal increases with increasing feed of HMABP.

As expected, the typical signal for aromatic protons in the region of 6.8–7.9 ppm shows an increase in intensity with increasing initial comonomer content. Depending on the used comonomer amount, also the intensity of the signal corresponding to the ^{i}Pr-group of NIPAM (3.7–4.3 ppm) changes. Consequently a higher integral ratio is obtained with increasing initial amount of HMABP. As shown in Table 3, the initial amount of HMBAP was almost completely incorporated into the polymer network.

3.2 Microgel properties

Size and structure. The effect of HMABP incorporation on the microgel particles in the collapsed state was investigated with SAXS measurements at $T = 40$ °C. Fig. 4 shows the SAXS-curves, which were obtained for each sample.

All curves show characteristic oscillations for spherical particles and could be fitted very precisely with a homogeneous sphere model (see eqn (4)) with a Gaussian radius distribution to account for polydispersity.[57] From the fits we extracted the radius of the microgel particles and their respective polydispersity. The data are presented in Table 4. The development of the radius can also be seen in the q-value of the first minimum of the SAXS curves. An increase of the HMABP content from 2 mol% to 4 mol% leads to a shift of the minimum to higher q-values, indicating a slight decrease in particle size. A further increase to 9 mol% seems to switch the position back to the initial value. This increase in size can be attributed to the increase of the initial mass content of the synthesis, as the amount of NIPAM and BIS were kept constant and only the amount of HMABP was varied during the syntheses. This was also observed by Kratz *et al.*[63] when they investigated PNIPAM-microgels with different cross-linker contents. For a HMABP content of 12 mol% the first minima is shifted back to higher values, connected to a decrease in particle size. Taking into account the obtained results, a comparison of all extracted radii depicted in Table 4 shows, that an increase of the HMABP content from 2 mol% to 12 mol% leads to a decrease of the particle radius from 46 nm to 40 nm. However, the

Table 3 Summary of the calculated incorporation for the HMABP-comonomer in the respective microgels, determined by ^{1}H-NMR spectroscopy

Sample	HMABP feed (mol%)	Incorporated HMABP content (mol%)
NcHMABP2.5	2.5	2.0
NcHMABP5	5.0	4.0
NcHMABP10	10.0	9.0
NcHMABP15	15.0	12.0

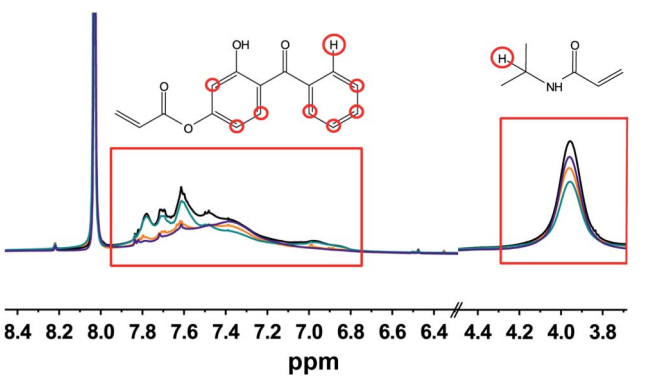

Fig. 3 ^{1}H-NMR spectra of the microgels with 2.5 mol% (purple), 5 mol% (orange), 10 mol% (turquoise) and 15 mol% (black) initial comonomer content. The measurements were performed in DMF-d_7 (peak at 8 ppm). The signals of the associated protons (red circles) are marked with red boxes.

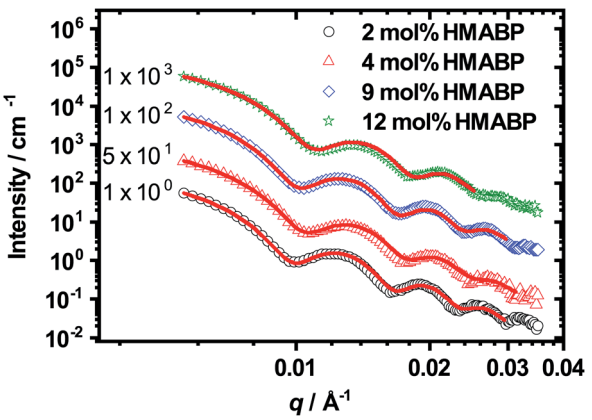

Fig. 4 SAXS data for collapsed microgels with different HMABP contents measured at 40 °C. The solid line is the fit to the experimental data using SasView. For better visibility in log scale, the curves are shifted with respect to each other by multiplying with multiples of 10.

Table 4 Summary of the results from the SAXS measurements for radius R and polydispersity PD determined by homogeneous sphere model for the respective microgels at 40 °C

Sample	R (nm)	PD (%)
NcHMABP2	46.2 ± 0.5	7.1 ± 1.6
NcHMABP4	43.2 ± 0.8	8.7 ± 1.3
NcHMABP9	45.6 ± 0.3	6.7 ± 1.7
NcHMABP12	40.1 ± 0.3	7.4 ± 1.2

polydispersity of all samples is rather independent of the HMABP content and is below 10% in all cases. In conclusion, we successfully synthesized spherical microgel particles, with low polydispersity and decreasing size with increasing HMABP content.

Swelling behaviour. To investigate the thermoresponsive behaviour of the obtained copolymer microgels, in dependence on the different comonomer amounts, temperature-dependent PCS measurements were performed. The obtained hydrodynamic radii of the investigated microgels and their swelling ratios α are shown as a function of temperature in Fig. 5. The swelling ratio α can be determined from the volume V of the particles in the swollen state and from the volume $V_{collapsed}$ of the shrunken state by means of eqn (5) with the assumption of spherical particles.

$$\alpha = \frac{V}{V_{collapsed}} = \frac{{R_h}^3}{{R_{h,collapsed}}^3} \quad (5)$$

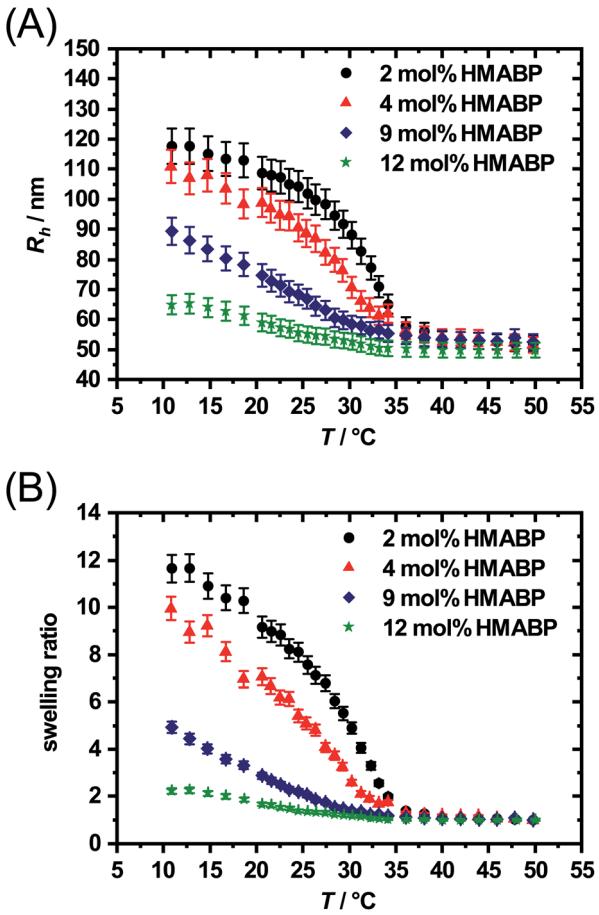

Fig. 5 Temperature-dependent particle sizes for microgels with different amounts of HMABP (A). For the determination of the VPTT the inflection point of the swelling curves was used. Due to the broadening of the phase transition with increasing the HMABP content, this point could not be defined precisely for all microgels. The swelling ratio as function of temperature (B).

In Fig. 5A it is clearly visible that the hydrodynamic radius of the microgel particles in the swollen state ($T = 10$ °C) decreases with increasing HMABP content while the hydrodynamic radius of the microgel particles in the collapsed state ($T = 50$ °C) is almost identical. The HMABP incorporation also shows an influence on the VPTT of the microgels. According to literature pure PNIPAM shows a volume phase transition temperature of *ca.* 33 °C.[20] The microgel particles with a comonomer content of 2 mol% exhibit a VPTT of 32 °C which is comparable to pure PNIPAM. However, if the comonomer content is increased to 4 mol% or more, a clear effect on the VPTT is evident. At 4 mol% HMABP the VPTT shifts to 30 °C. A further increase of the comonomer content to 9 mol% causes a broadening of the swelling transition and no well defined VPTT is observable. The microgel particles with a HMABP content of 12 mol% seem to completely loose their thermo-sensitivity. However, it cannot be ruled out that the network is still responsive on a very local length scale, which does not lead to changes in R_h.

The same trend of a VPTT shift to lower temperatures was observed by Hertle *et al.* for NIPAM-*co*-*tert*-butylacrylamide copolymer microgels (NIPAM-*co*-NtBAM).[35] This work attributed the effect to the hydrophobicity of NtBAM, which causes an increase of hydrophobicity in the whole polymer network compared to pure PNIPAM. Pure PNIPAM microgels show a rather narrow and steep change from the hydrophilic to the hydrophobic state, due to the presence of hydrophilic amide groups and the hydrophobic isopropyl group on the side chain. If now the amount of hydrophobic comonomer is increased, the hydrophobicity of the whole polymer network increases. Such an impact on the VPTT by incorporation of an acrylate as comonomer, as used in this work, has been observed in earlier work for *tert*-butylacrylate.[64]

Furthermore, a higher content of HMABP strongly reduces the swelling ratio of the microgel particles, as shown in Fig. 5B. Microgels with 2 mol% HMBAP show a maximum swelling ratio of 12. Microgel particles with a comonomer content of 4 mol% show a maximum swelling ratio of 10, which decreases to 5 at a comonomer content of 9 mol%. At a high comonomer content of 12 mol% there is practically no evidence for swelling behaviour, which is indicated by the low maximum swelling ratio of 2. The small temperature-dependent size change is likely to be osmotic swelling. All mentioned observations can be attributed to the hydrophobic comonomer incorporated in the polymer network. Hence, the incorporation of HMABP was successful as expected from the NMR measurements.

3.3 Investigation of free-standing microgel layers

Prior to the preparation of free-standing membranes, the microgel particles were transferred to a substrate by spin-

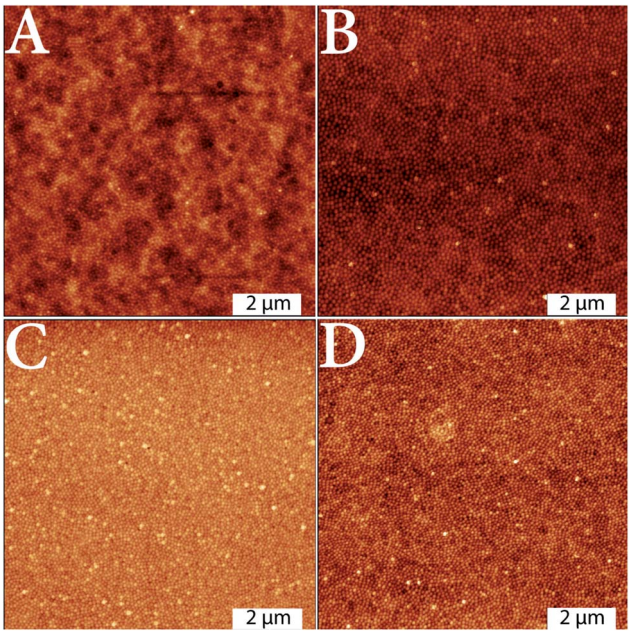

Fig. 6 AFM images (10 × 10 μm) of cross-linked microgel layers. Images of spin-coated microgel layers from the samples with 2 mol% (A), 4 mol% (B), 9 mol% (C) and 12 mol% (D) comonomer content. All layers were prepared using the spin-coating parameters, which are described in the Experimental section. The insert scale bar is 2 μm.

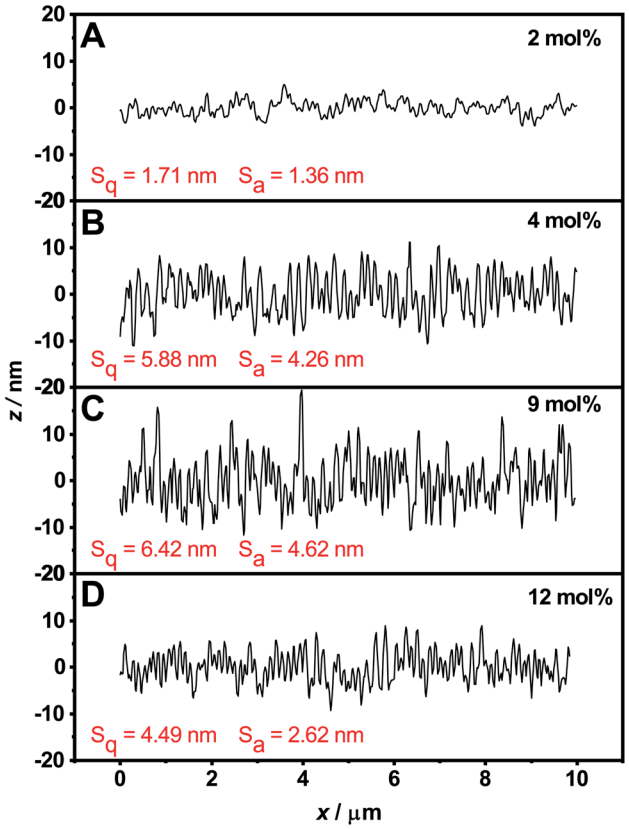

Fig. 7 Surface roughness in dependence of the comonomer content obtained from the AFM images of the cross-linked microgel layers (Fig. 6). Mean roughness S_a and mean square roughness S_q were calculated for an area of 100 μm^2 using the software Gwyddion.[59]

coating as described in the experimental part. In order to ensure a homogeneous cross-linking of the microgel particles, it is very important that the particles are packed very tightly and the resulting layers are rather smooth and do not have detectable holes. After the irradiation with UV light, the cross-linked microgel layers were analyzed by AFM (Fig. 6).

The AFM images of the cross-linked layers on the substrate in Fig. 6 show densely packed microgel particles. During the preparation several microgel layers were deposited on the substrate. As a consequence of the deposition of multiple layers, all samples show a very high packing density, far above the 2 dimensional hexagonal close packing which is usually achieved by spin-coating (Fig. 6). Also the height of the layer shows some inhomogeneities at sections where microgel multilayers are obtained. For the microgel particles with a low comonomer content (2 mol%) the inhomogeneities seem to be most prominent, while they decrease upon increase of comonomer content. This may be connected to a smaller particle size, which was already shown by the SAXS and PCS measurements.

For a more detailed consideration of the surface properties, the surface roughness for the respective layers was also determined from the AFM images using the software Gwyddion[59] (Fig. 7). Values for the mean roughness S_a, which describes the height irregularities, and the corresponding mean square roughness S_q (RMS) were obtained. Compared to the visual impression, the calculated values show the lowest surface roughness for the layer of microgels with the lowest comonomer content (S_a = 1.36 nm, S_q = 1.71 nm). For the layers of microgels with comonomer contents of 4 mol% (S_a = 4.26 nm, S_q = 5.88 nm) and 9 mol% (S_a = 4.62 nm, S_q = 6.42 nm), a steady increase in surface roughness is observed. The layer with the highest comonomer content is again smoother (S_a = 2.62 nm, S_q = 4.49 nm), but still exhibits a higher surface roughness than the layer with the lowest comonomer content. Despite the differences in surface roughness, the roughness values are quite low, so that the layers analyzed here can still be regarded as smooth with respect to the thickness.

In order to determine the average layer thickness of the cross-linked layers, ellipsometry measurements were performed. Due to repeated spin-coating of the particles the layer thickness of all cross-linked layers is between 195 nm and 285 nm in the dry state, which corresponds to a deposition of only 2–3 layers of microgels on the substrate. From the AFM measurements, which showed a very dense packing of the

Table 5 Layer thicknesses of the cross-linked microgel layers with different comonomer contents, determined by ellipsometry in the dry state.

Sample name	Layer thickness/nm
NcHMABP2	255 ± 6.4
NcHMABP4	220 ± 6.4
NcHMABP9	195 ± 4.8
NcHMABP12	285 ± 6.8

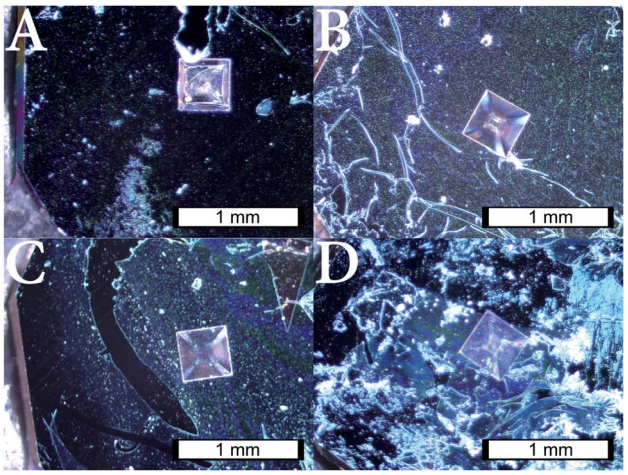

Fig. 8 Photograph of cross-linked microgel layers deposited on a funnel hole of a Si_3N_4-chip after detachment from a silicon wafer. The membranes are made of cross-linked microgels containing 2 mol% (A), 4 mol% (B), 9 mol% (C) and 12 mol% (D) HMABP. The chips containing the microgel membranes were used in this form for the resistance measurements. The insert scale bar is 1 mm.

microgels and the layer thickness determined by ellipsometry, we expect the cross-linked layers to be stable enough to form free-standing membranes. The results of the specific layer thicknesses for the respective cross-linked microgel particles are summarized in Table 5.

After the detachment of the layers, the microgel membrane slowly floats from the wafer towards the air/liquid interface, where the microgel membrane can be picked up and transferred to any substrate. As an experiment demonstrating the potential of free-standing microgel membranes and investigating the thermoresponsive property of cross-linked free-standing microgel films, the detached membranes were transferred to a Si_3N_4-chip with a 200 × 200 μm funnel hole (Fig. 8). As it can be seen in Fig. 8, the funnel hole is completely spanned with membranes containing 2 mol% (A), 4 mol% (B), 9 mol% (C) and 12 mol% (D) HMABP. Fig. 8 also shows, that the mechanical stability of the membrane is high enough to transfer it to the Si_3N_4-chip without ruptures.

3.4 Resistance measurements

To show the reversible temperature-dependent switching of the membranes, resistance measurements with increasing and decreasing temperature were performed, as shown in Fig. 9. As can be seen, the resistance at low temperatures is for all membranes about 250 kΩ. Here, the cross-linked microgel particles are in a swollen state, which is illustrated by the additionally plotted swelling curve (green). However, with increasing temperature the resistance of the membrane initially remains constant until a sharp increase of the membrane resistance is observable at a temperature of 33 °C. A further increase of the temperature does not increase the measured resistance further, which leads to a plateau. Interestingly, the steep increase in membrane resistance seems to be connected to the VPTT of PNIPAM, which is around 33 °C [20] in all cases

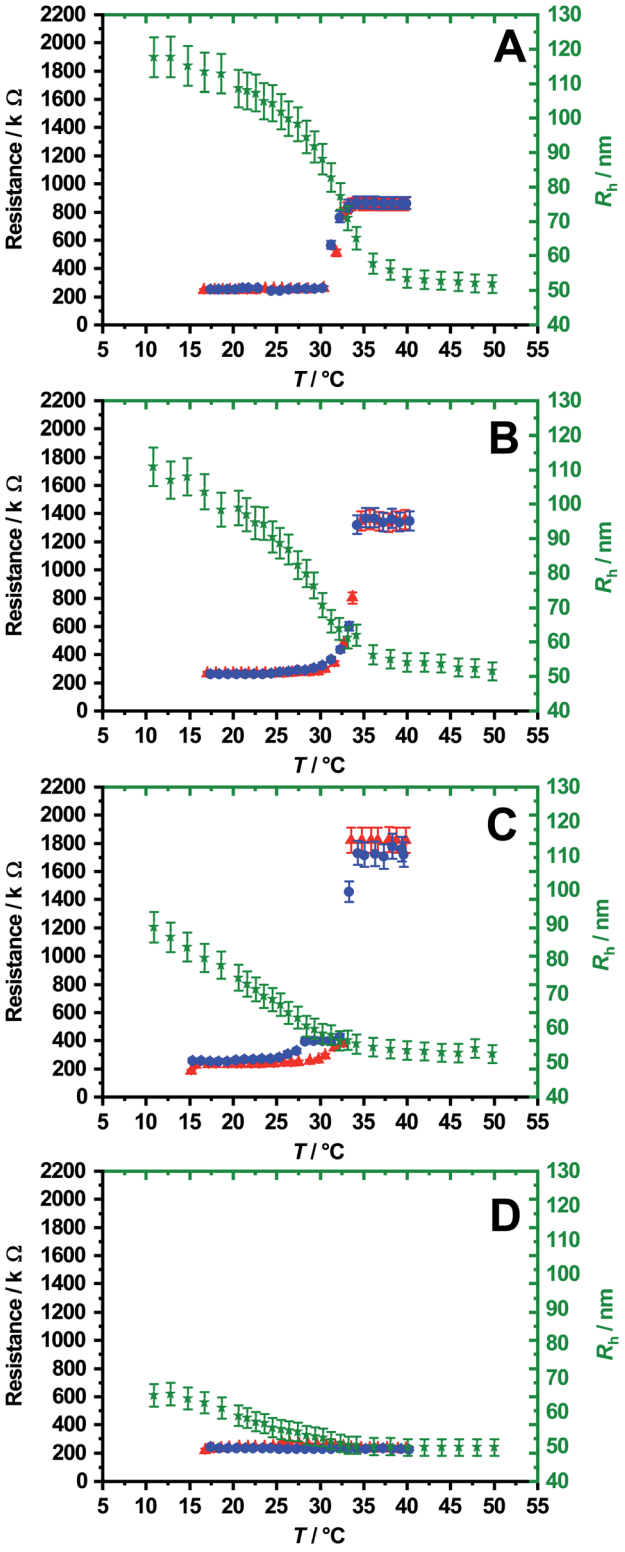

Fig. 9 Resistance as a function of temperature for membranes with 2 mol% (A), 4 mol% (B), 9 mol% (C) and 12 mol% (D) comonomer content. In each case a measuring cycle is shown which consists of a heating curve (red) and a cooling curve (blue). Additionally the swelling curve (green) of the corresponding microgels obtained from PCS measurements is plotted. Due to the low swelling capacity and the loss of a real thermoresponse in (D) no effect is observed. In all other cases drastic increases of the resistance occur at the VPTT.

except for the membranes produced with microgels containing 12 mol% HMABP. Here neither the membrane nor the microgel particles show a significant thermoresponsive behaviour. In the plateau region, which corresponds to the fully collapsed particles, the membranes reveal different resistances with increasing comonomer content. Microgels with a comonomer content of 2 mol% show a resistance of 900 kΩ. This increases to 1.4 MΩ at 4 mol% comonomer content and a resistance of 1.8 MΩ is reached at 9 mol% comonomer content. We suspect that the differences in resistance are attributable on the one hand to the slightly different layer thickness of the membranes and on the other hand to the increase of the multiple cross-linking points between the microgel particles of the membrane with increasing comonomer content. In fact, the switching point of the membranes is very sharp in comparison to the corresponding swelling curve and independent of the comonomer content. The collapse of the cross-linked microgel particles and thus the sharp transition, occurs always at the VPTT of PNIPAM. Whereas, in the swelling curves an increasing comonomer content leads to broadening of the phase transition and the VPTT of the microgel is shifted to lower temperatures. We suppose, that the switching of the membrane is not necessarily connected to the size change of the microgel particles. Instead it can be explained by the local interactions between the polymer network and the solvent. Before reaching the VPTT of PNIPAM, the network has hydrophilic properties on a local scale, while polymer/polymer interactions are dominant above this temperature. Hence, the diffusion of the ions changes strongly, when the network properties are switched between these two states. Above the VPTT of PNIPAM, the network forms a diffusion barrier for the polar ions, while the membrane in the swollen state does not provide a sufficient barrier to hinder the diffusion of those.

If the free-standing microgel membranes presented here are compared with membranes investigated by Frost *et al.*,[38] Menne *et al.*,[15] or Bell *et al.*,[45] it becomes clear that they show a different switching behaviour. Most importantly, there is a significant difference in the preparation and nature of the membranes in which a template has always been used and modified with microgels *via* dynamic adsorption or NIPAM was attached to a PET membrane by FRP and ATRP.[15,38,65] In the work of Bell *et al.* a very thick multilayer is produced by photo-crosslinking a microgel filter cake on a polymer filter-membrane. In contrast to the ones shown here, all these membranes exhibit the highest resistance and the highest retention at low temperatures which corresponds to the swollen state of the microgels or the used linear chains.[45]

As the temperature increases, the network of the microgels collapse at the VPTT and the resistance decreases. Frost *et al.*[38] call this a positive switching effect in which the permeability increases with increasing temperature. Furthermore, when investigating PNIPAM grafted membranes with large (320 nm) and small (80 nm) pores, Alem *et al.*[65] showed that these membranes exhibit opposite conductivity behaviour. For membranes with large pores, the conductivity increases with increasing temperature. In contrast, membranes with small pores exhibit the opposite behaviour.

For large pores, the thickness of the polymer brushes in the swollen state is equal to the virgin pore size (330 nm), so below the VPTT the extended chains block the pores and thus reduce the effective pore size, which is reflected in low conductivity. As the temperature rises, the chains collapse and release the pores, while an increase in conductivity is detected. In the case of narrow pore membranes, the layer thickness of the swollen PNIPAM layers (135–250 nm) is greater than the pore size of the membrane (80 nm). Although the pores are completely covered with the extended PNIPAM brushes at low temperatures, high permeability is detected due to the high hydration of the chains. If the chains collapse, the pores are completely blocked and the diffusion of ions is prevented. Alem *et al.* attribute this behaviour to formation of microgel membranes, which are also studied in this work. As already mentioned earlier, the authors call this a negative switching effect.

3.5 Free-standing catalytic films

Firstly we investigated if the synthesis of silver nanoparticles inside the network of the copolymer microgel particles was successful. Therefore, dry state TEM measurements were performed on non cross-linked microgel particles. The results are shown in Fig. 10.

It is clearly observable that the microgel particles exhibit different levels of loading with silver nanoparticles. Some of the microgels are decorated strongly, while others seem to be loaded with one or two particles, only. Also, some of the microgel particles are empty and do not show a decoration with silver nanoparticles. A result like this could be expected as no stabilizing comonomer like acrylic acid was used in the present microgels.[66] Because of that some nanoparticles, which are not trapped inside the polymer network, bleed during the purification of the samples. But in fact, most of the microgels are decorated with silver nanoparticles and because of that it is very likely that the formation

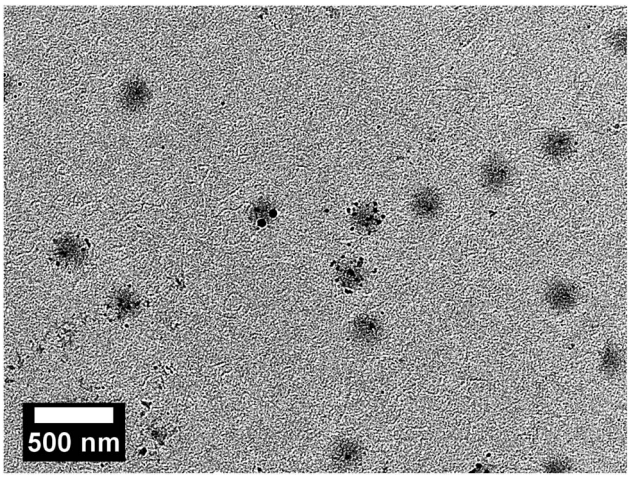

Fig. 10 Dry state TEM image of P(NIPAM-*co*-HMABP) microgels with a comonomer content of 4 mol% decorated with silver nanoparticles. In addition to silver nanoparticles incorporated into the microgels, individual nanoparticles can also be detected outside the polymer network, which can be attributed to the "bleeding" of the nanoparticles out of the microgel network.

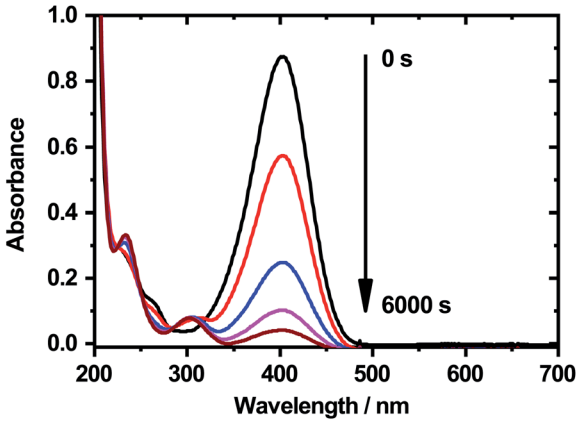

Fig. 11 Absorbance spectra of 4-nitrophenol during the catalytic reduction with $NaBH_4$ in presence of the free-standing catalytic membrane. The measurements were performed after a reaction time of 0 s (black), 1000 s (red), 2000 s (blue), 3000 s (magenta) and 6000 s (brown) at a temperature of 311 K.

a free-standing membrane out of the silver nanoparticle decorated microgels will lead to a catalytic membrane as well.

After the UV cross-linking of those particles, the catalytic activity of the free-standing membranes was investigated by following the reduction of 4-nitrophenol with $NaBH_4$ with UV/Vis spectroscopy. This model reaction is the most prominent example for the determination of the catalytic activity of nanoparticles embedded in different carrier systems.[67] Fig. 11 shows the absorbance spectra, which were recorded during the measurements.

It is clearly visible, that the absorbance maximum at 400 nm decreases strongly with increasing reaction time. This indicates, that the silver nanoparticles located inside of the catalytic film still show a significant catalytic activity. It is to mention that the reaction rate for the reduction is extremely slow, compared to colloidal nanoreactor particles which are not cross-linked to a membrane,[68,69] but in this case the catalyst is of course not distributed homogeneously inside the whole reaction vessel, which influences the reaction rate a lot. In addition, the amount of incorporated silver nanoparticles in the microgels is significantly lower compared to the work of Lu *et al.*[32,70] and Pich *et al.*,[68] which also results in lower catalytic activity as it correlates with the concentration of silver nanoparticles inside the polymer network.

However, it can be stated that the silver nanoparticle decorated free-standing membranes are suitable catalysts for the reduction of 4-nitrophenol. This offers an interesting perspective for future investigations, for example on the switchability of the catalytic activity or the design of intelligent flow-through microfluidic devices for catalytic reactions.

4 Conclusions

In this work we present the synthesis of PNIPAM-*co*-HMABP microgels and their subsequent cross-linking by UV-light. This leads to the formation of free-standing transferable membranes which are still thermoresponsive up to 9 mol% of the HMABP comonomer. Moreover, we show that these membranes can be used to regulate ion flow and the resistance increases by up to nearly one order of magnitude upon heating the membrane beyond the VPTT. This is an important step towards self-regulating membranes with applications *e.g.* in fuel cells or water purification systems.

In addition this work reveals that the same approach can also be used to cross-link nanoparticle carrying microgels leading to free-standing membranes with catalytic activity.

Conflicts of interest

There are no conflicts to declare.

Acknowledgements

The authors thank the DFG for financial support within the projects HE2995/6-1, INST 215/432-1 FUGG. This work benefited from the use of the SasView application, originally developed under NSF award DMR-0520547. SasView contains code developed with funding from the European Union's Horizon 2020 research and innovation program under the SINE2020 project, grant agreement no. 654000. We acknowledge support for the publication costs by the Open Access Publication Fund of Bielefeld University.

Notes and references

1 J. R. Varcoe, R. C. T. Slade, E. Lam How Yee, S. D. Poynton, D. J. Driscoll and D. C. Apperley, *Chem. Mater.*, 2007, **19**, 2686–2693.
2 K. Wang, A. A. Abdalla, M. A. Khaleel, N. Hilal and M. K. Khraisheh, *Desalination*, 2017, **401**, 190–205.
3 Z.-X. Lu, A. Namboodiri and M. M. Collinson, *ACS Nano*, 2008, **2**, 993–999.
4 I. Lokuge, X. Wang and P. W. Bohn, *Langmuir*, 2007, **23**, 305–311.
5 V. Papaefthimiou, R. Steitz and G. Findenegg, *Chem. Unserer Zeit*, 2008, **42**, 102–115.
6 X. Zhang, C. Neumann, P. Angelova, A. Beyer and A. Gölzhäuser, *Langmuir*, 2014, **30**, 8221–8227.
7 J. Li and D. J. Mooney, *Nat. Rev. Mater.*, 2016, **1**, 16071.
8 J. C. T. Eijkel and A. van den Berg, *Lab Chip*, 2006, **6**, 19–23.
9 W. J. Koros and G. K. Fleming, *J. Membr. Sci.*, 1993, **83**, 1–80.
10 R. W. Baker, *Ind. Eng. Chem. Res.*, 2002, **41**, 1393–1411.
11 E. Kharlampieva, V. Kozlovskaya and S. A. Sukhishvili, *Adv. Mater.*, 2009, **21**, 3053–3065.
12 H. Kanazawa, K. Yamamoto, Y. Matsushima, N. Takai, A. Kikuchi, Y. Sakurai and T. Okano, *Anal. Chem.*, 1996, **68**, 100–105.
13 Q. Wu, R. Wang, X. Chen and R. Ghosh, *J. Membr. Sci.*, 2014, **471**, 56–64.
14 K. Uhlig, T. Wegener, Y. Hertle, J. Bookhold, M. Jaeger, T. Hellweg, A. Fery and C. Duschl, *Polymers*, 2018, **10**, 656.
15 D. Menne, F. Pitsch, J. E. Wong, A. Pich and M. Wessling, *Angew. Chem., Int. Ed.*, 2014, **53**, 5706–5710.

16 F. A. Plamper and W. Richtering, *Acc. Chem. Res.*, 2017, **50**, 131–140.
17 J. A. Bonham, M. A. Faers and J. S. van Duijneveldt, *Soft Matter*, 2014, **10**, 9384–9398.
18 W. Richtering and B. R. Saunders, *Soft Matter*, 2014, **10**, 3695.
19 M. Karg, A. Pich, T. Hellweg, T. Hoare, L. A. Lyon, J. J. Crassous, D. Suzuki, R. A. Gumerov, S. Schneider, I. I. Potemkin and W. Richtering, *Langmuir*, 2019, **35**, 6231–6255.
20 C. Wu and S. Zhou, *J. Polym. Sci., Part B: Polym. Phys.*, 1996, **34**, 1597–1604.
21 S. Nayak, D. Gan, M. J. Serpe and L. A. Lyon, *Small*, 2005, **1**, 416–421.
22 M. J. Serpe, K. A. Yarmey, C. M. Nolan and L. A. Lyon, *Biomacromolecules*, 2005, **6**, 408–413.
23 Z. Wang, Y. Li, L. Chen, X. Xin and Q. Yuan, *J. Agric. Food Chem.*, 2013, **61**, 5880–5887.
24 S. Lehmann, S. Seiffert and W. Richtering, *J. Colloid Interface Sci.*, 2014, **431**, 204–208.
25 Y. Zhang and A. L. Yarin, *J. Mater. Chem.*, 2009, **19**, 4732.
26 B. Sung, C. Kim and M.-H. Kim, *J. Colloid Interface Sci.*, 2015, **450**, 26–33.
27 M. Dirksen, C. Dargel, L. Meier, T. Brändel and T. Hellweg, *Colloid Polym. Sci.*, 2020, **298**, 505–518.
28 Y. Matsumura and K. Iwai, *Polymer*, 2005, **46**, 10027–10034.
29 K. Iwai, Y. Matsumura, S. Uchiyama and A. P. d. Silva, *J. Mater. Chem.*, 2005, **15**, 2796.
30 M. Karg and T. Hellweg, *Curr. Opin. Colloid Interface Sci.*, 2009, **14**, 438–450.
31 Y. Mei, Y. Lu, F. Polzer, M. Ballauff and M. Drechsler, *Chem. Mater.*, 2007, **19**, 1062–1069.
32 Y. Lu, Y. Mei, M. Ballauff and M. Drechsler, *J. Phys. Chem. B*, 2006, **110**, 3930–3937.
33 K. Kratz and W. Eimer, *Berichte der Bunsengesellschaft für physikalische Chemie*, 1998, **102**, 848–854.
34 T. Hoare and R. Pelton, *Macromolecules*, 2004, **37**, 2544–2550.
35 Y. Hertle, M. Zeiser, C. Hasenöhrl, P. Busch and T. Hellweg, *Colloid Polym. Sci.*, 2010, **288**, 1047–1059.
36 K. Uhlig, T. Wegener, J. He, M. Zeiser, J. Bookhold, I. Dewald, N. Godino, M. Jaeger, T. Hellweg, A. Fery and C. Duschl, *Biomacromolecules*, 2016, **17**, 1110–1116.
37 S. Schmidt, M. Zeiser, T. Hellweg, C. Duschl, A. Fery and H. Möhwald, *Adv. Funct. Mater.*, 2010, **20**, 3235–3243.
38 S. Frost and M. Ulbricht, *J. Membr. Sci.*, 2013, **448**, 1–11.
39 R. Bernstein, E. Antón and M. Ulbricht, *J. Membr. Sci.*, 2013, **427**, 129–138.
40 M. Barth, M. Wiese, W. Ogieglo, D. Go, A. Kuehne and M. Wessling, *J. Membr. Sci.*, 2018, **555**, 473–482.
41 I. V. Portnov, M. Möller, W. Richtering and I. I. Potemkin, *Macromolecules*, 2018, **51**, 8147–8155.
42 M. Wiese, T. Lohaus, J. Haussmann and M. Wessling, *J. Membr. Sci.*, 2019, **588**, 117190.
43 C. Cutright, R. Finkelstein, E. Orlowski, E. McIntosh, Z. Brotherton, T. Fabiani, S. Khan, J. Genzer and S. Menegatti, *J. Membr. Sci.*, 2020, **616**, 118439.
44 L. Wu and E. Sancaktar, *J. Membr. Sci.*, 2020, **610**, 118304.
45 D. Bell, S. Ludwanowski, A. Lüken, B. Sarikaya, A. Walther and M. Wessling, *J. Membr. Sci.*, 2021, **620**, 118912.
46 S. Wellert, M. Richter, T. Hellweg, R. v. Klitzing and Y. Hertle, *J. Phys. Chem.*, 2015, **229**, 7–8.
47 J. Bookhold, M. Dirksen, L. Wiehemeier, S. Knust, D. Anselmetti, F. Paneff, X. Zhang, A. Gölzhäuser, T. Kottke and T. Hellweg, *Soft Matter*, 2021, **17**, 2205–2214.
48 A. Turchanin and A. Gölzhäuser, *Adv. Mater.*, 2016, **28**, 6075–6103.
49 S. Koch, C. D. Kaiser, P. Penner, M. Barclay, L. Frommeyer, D. Emmrich, P. Stohmann, T. Abu-Husein, A. Terfort, D. H. Fairbrother, O. Ingólfsson and A. Gölzhäuser, *Beilstein J. Nanotechnol.*, 2017, **8**, 2562–2571.
50 S. Aftab, M. F. Khan, P. Gautam, H. Noh and J. Eom, *Nanoscale*, 2019, **11**, 9518–9525.
51 S. Aftab, I. Akhtar, Y. Seo and J. Eom, *ACS Appl. Mater. Interfaces*, 2020, **12**, 42007–42015.
52 S. Aftab, M. Samiya, K. Rabia, S. Yousuf, M. U. Khan, R. Khawar, A. Younus, M. Manzoor, M. W. Iqbal and M. Z. Iqbal, *Nanoscale*, 2020, **12**, 15687–15696.
53 S. Aftab, M. Samiya, M. W. Iqbal, P. A. Shinde, A. U. Rehman, S. Yousuf, S. Park and S. C. Jun, *Nanoscale*, 2020, **12**, 18171–18179.
54 R. Pelton, *Adv. Colloid Interface Sci.*, 2000, **85**, 1–33.
55 S. W. Provencher, *Comput. Phys. Commun.*, 1982, **27**, 229–242.
56 F. Zhang, J. Ilavsky, G. G. Long, J. P. G. Quintana, A. J. Allen and P. R. Jemian, *Metall. Mater. Trans. A*, 2010, **41**, 1151–1158.
57 http://www.sasview.org/.
58 A. Guinier, G. Fournet, C. Walker and G. Vineyard, *Small-Angle Scattering of X-Rays*, JOHN WILEY & SONS, Inc., 1955.
59 D. Necas and P. Klapetek, *Cent. Eur. J. Phys.*, 2012, **10**, 181–188.
60 D. Beaglehole, *Physica B+C*, 1980, **100**, 163–174.
61 D. Bonn, *Europhys. Lett.*, 1992, **20**, 235–239.
62 S. Schmidt, H. Motschmann, T. Hellweg and R. v. Klitzing, *Polymer*, 2008, **49**, 749–756.
63 K. Kratz, T. Hellweg and W. Eimer, *Polymer*, 2001, **42**, 6631–6639.
64 Q.-S. Zhang, L.-S. Zha, J.-H. Ma and B.-R. Liang, *J. Appl. Polym. Sci.*, 2007, **103**, 2962–2967.
65 H. Alem, A.-S. Duwez, P. Lussis, P. Lipnik, A. M. Jonas and S. Demoustier-Champagne, *J. Membr. Sci.*, 2008, **308**, 75–86.
66 B. Naik, S. Hazra, P. Muktesh, V. S. Prasad and N. N. Ghosh, *Sci. Adv. Mater.*, 2011, **3**, 1025–1030.
67 Y. Lu and M. Ballauff, *Prog. Polym. Sci.*, 2011, **36**, 767–792.
68 A. Pich, A. Karak, Y. Lu, A. K. Ghosh and H.-J. P. Adler, *Macromol. Rapid Commun.*, 2006, **27**, 344–350.
69 Y. Lu, S. Proch, M. Schrinner, M. Drechsler, R. Kempe and M. Ballauff, *J. Mater. Chem.*, 2009, **19**, 3955.
70 Y. Lu, Y. Mei, M. Drechsler and M. Ballauff, *Angew. Chem., Int. Ed. Engl.*, 2006, **45**, 813–816.